PHYSICAL REVIEW RESEARCH **6**, L032036 (2024)

Letter

Ultra-high-amplitude Peregrine solitons induced by helicoidal spin-orbit coupling

Cui-Cui Ding,[1] Qin Zhou,[1,2,*] and B. A. Malomed[3,4]

[1]*Research Group of Nonlinear Optical Science and Technology, Research Center of Nonlinear Science, School of Mathematical and Physical Sciences, Wuhan Textile University, Wuhan 430200, China*

[2]*State Key Laboratory of New Textile Materials and Advanced Processing Technologies, Wuhan Textile University, Wuhan 430200, China*

[3]*Department of Physical Electronics, School of Electrical Engineering, Faculty of Engineering, and the Center for Light-Matter University, Tel Aviv University, Tel Aviv, Israel*

[4]*Instituto de Alta Investigación, Universidad de Tarapacá, Casilla 7D, Arica, Chile*

(Received 10 April 2024; accepted 31 July 2024; published 13 August 2024)

In the framework of the model of a spatially nonuniform Bose-Einstein condensate with helicoidal spin-orbit (SO) coupling, we find abnormal Peregrine solitons (PSs) on top of flat and periodic backgrounds, with ultrahigh amplitudes. We explore the roles of the SO coupling strength and helicity pitch in the creation of these anomalously tall PSs and find that their amplitude, normalized to the background height, attains indefinitely large values. The investigation of the modulation instability (MI) in the same system demonstrates that these PSs exist in a range of relatively weak MI, maintaining the feasibility of their experimental observation.

DOI: 10.1103/PhysRevResearch.6.L032036

Introduction. Rogue waves (RWs), first discovered as extreme events in the ocean [1–6], have been widely studied, due to their unique properties and potential applications in nonlinear optics [7–10], plasmas [11], Bose-Einstein condensates (BECs) [12–14], magnetics [15], financial markets [16], and various other settings [17–26]. A widely recognized RW prototype is provided by the exact Peregrine-soliton (PS) solution of the nonlinear Schrödinger equation (NLSE) [27], whose characteristic features are the threefold peak amplitude and spatiotemporal localization on top of the background field [28]. Several landmark experiments have directly demonstrated this remarkable phenomenon and its ramifications [14,28–30].

Spin-orbit (SO) coupling in BECs have drawn much interest since its experimental implementation [31–33], as it offers the realization of the SO-coupling phenomenology in the uniquely clean form [34,35] and make it possible to create artificial vector gauge potentials [36,37]. Recently, models of BECs with nonuniform SO coupling have been introduced, as they provide high tunability of this effect, and enhance the role of the intrinsic nonlinearity in the SO-coupled BECs [38–43]. In this context, soliton dynamics in the BEC with nonuniform landscapes of the SO coupling has been investigated [44–47], where, in particular, the helicoidal gauge potential may originate from the light propagation in a helical waveguide array [48]. The propagation of matter-wave solitons in a BEC with a random SO coupling was addressed, too [49].

*Contact author: qinzhou@whu.edu.cn

SO-coupled BECs are modeled by systems of two (or several) coupled Gross-Pitaevskii equations (GPEs). In this connection, it is relevant to stress that PSs exist in multicomponent NLSE models, such as the famous Manakov system, but, due to the energy transfer between different components, the PS amplitude is no longer fixed, although it still does not exceed the triple background height [24,50,52,53]. Nevertheless, recent studies have shown that, under the action of self-steepening effects, the amplitude of fundamental PSs can exceed the threefold limit, reaching up to fivefold the background height [54]. In particular, exceptional PSs, which feature ultra-high peak amplitudes, have also been reported in the vector derivative NLSEs, including the self-steepening effect [55].

In this work, we focus on the following questions: can the fundamental PS with an ultrahigh peak amplitude be excited in other ways, besides using higher-order effects, such as self-steepening, and to what extent is it possible to increase the PS amplitude? To answer these questions, we first consider a BEC model with nonuniform helicoidal SO coupling (cf. Ref. [44]), which offers experimental feasibility. We construct its exact fundamental PS solutions on top of flat, alias continuous-wave (CW), and periodic backgrounds. Through the analysis of the PS amplitude, we find that PS with ultrahigh peak amplitude, reaching indefinitely large values (as normalized to the background height), can be created with the help of the helicoidal SO coupling.

To explore the PS dynamics under the action of spatially nonuniform gauge potentials, we consider the GPE for the spinor wave function $\mathbf{\Psi} = (\Psi_1, \Psi_2)^T$ of an effectively one-dimensional two-component BEC, including the helicoidal SO coupling. In the scaled form (with $M = \hbar = 1$, where M is the atomic mass), the GPE is [44,56,57]

$$i\frac{\partial \mathbf{\Psi}}{\partial t} = \frac{1}{2}Q^2(x)\mathbf{\Psi} - (\mathbf{\Psi}^\dagger\mathbf{\Psi})\mathbf{\Psi}, \tag{1}$$

where the helicoidally molded SO coupling is represented by the generalized momentum operator,

$$Q(x) = -i\partial_x + \alpha\boldsymbol{\sigma}\cdot\boldsymbol{n}(x). \tag{2}$$

Here α is the SO-coupling strength, which is tunable in the experiment [39–41], $\boldsymbol{\sigma} = (\sigma_x, \sigma_y, \sigma_z)$ is the vector of the Pauli matrices, and the spatial modulation is represented by vector

$$\boldsymbol{n}(x) = (\cos(2\kappa x), \sin(2\kappa x), 0), \tag{3}$$

with $\kappa < 0$ and $\kappa > 0$ corresponding to the left- and right-handed helicity, respectively [48,58,59]. As usual, it is assumed that the inter and intraspecies attractive interactions have equal strengths. Special forms of Eq. (1) include the uniform Rashba-Dresselhaus SO coupling [36] when $\kappa = 0$, and the canonical Manakov system [50] when $\alpha = 0$.

Fundamental PS solutions. Equation (1) is made gauge equivalent to the integrable Manakov system,

$$i\mathbf{u}_t + \tfrac{1}{2}\mathbf{u}_{xx} + (\mathbf{u}^\dagger\mathbf{u})\mathbf{u} = 0, \quad \mathbf{u} = (u_1, u_2)^T, \tag{4}$$

by means of the transformation [49]

$$\boldsymbol{\Psi} = \begin{pmatrix} \nu_+ e^{-i(k_\mathrm{m}+\kappa)x} & \nu_- e^{i(k_\mathrm{m}-\kappa)x} \\ \nu_- e^{-i(k_\mathrm{m}-\kappa)x} & -\nu_+ e^{i(k_\mathrm{m}+\kappa)x} \end{pmatrix}\mathbf{u}, \tag{5}$$

where $k_\mathrm{m} = \sqrt{\alpha^2+\kappa^2}$ is the effective momentum of the lowest-energy states, and

$$\nu_+ = \mathrm{sgn}(\alpha)\sqrt{(k_\mathrm{m}-\kappa)/(2k_\mathrm{m})}, \tag{6}$$

$$\nu_- = \sqrt{(k_\mathrm{m}+\kappa)/(2k_\mathrm{m})}. \tag{7}$$

Below, k_m plays a crucial role determining properties of PSs, especially as concerns the amplification of their amplitudes.

The Manakov system (4) possesses the Lax pair [51] and admits the solution by means of the Darboux dressing method [24]. To begin with, we take the CW seed solution of Manakov system (4), with components

$$u_{j0} = a\exp[-i(k_j x - \omega_j t)], \quad j = 1, 2, \tag{8}$$

which is determined by the amplitude (a), wavenumbers (k_j), and frequencies

$$\omega_j = 2a^2 - k_j^2/2. \tag{9}$$

Making use of the Manakov system invariance with respect to the rotation of the set of the two components, we choose them in Eq. (8) with equal amplitudes a. Subsequent results demonstrate that the helicoidal SO coupling makes PS heights different in the two components $\Psi_{1,2}$ for the same background amplitudes a, see Eqs. (13) and (15) below.

Utilizing the known PS solutions for Manakov system (4) derived by means of the Darboux transform [24], and substitution (5), we obtain the following exact fundamental PS solutions of the underlying Eq. (1):

$$\begin{aligned}
\Psi_1 &= ae^{-i\kappa x}\left[\nu_+\left(1-\frac{\mathcal{R}_1}{\mathcal{N}_1}\right)e^{i\theta_1} + \nu_-\left(1-\frac{\mathcal{R}_2}{\mathcal{N}_2}\right)e^{i\theta_2}\right],\\
\Psi_2 &= ae^{i\kappa x}\left[\nu_-\left(1-\frac{\mathcal{R}_1}{\mathcal{N}_1}\right)e^{i\theta_1} - \nu_+\left(1-\frac{\mathcal{R}_2}{\mathcal{N}_2}\right)e^{i\theta_2}\right], \qquad (10)\\
\theta_1 &= -(k_\mathrm{m}+k_1)x + \omega_1 t, \quad \theta_2 = (k_\mathrm{m}-k_2)x + \omega_2 t,
\end{aligned}$$

where we define

$$\begin{aligned}
\mathcal{N}_j &= \left[(\theta+\mu t)^2 + \zeta^2 t^2 + \frac{4}{\zeta^2}\right]\{[\delta + (-1)^j\mu]^2 + \zeta^2\},\\
\mathcal{R}_j &= 8i\{\zeta^2 t - [\mu + (-1)^j\delta](\theta+\mu t)\} + 16, \qquad (11)\\
\mu &= \pm\frac{\sqrt{2}}{2}[\sqrt{\delta^2(8a^2+\delta^2)} - 4a^2 + \delta^2]^{1/2}
\end{aligned}$$

in the case of $|\delta| \geqslant a$, with $\delta \equiv k_1 - k_2$, or

$$\begin{aligned}
\mathcal{N}_j &= \left[\theta^2 + (\zeta+\mu')^2 t^2 + \frac{4}{(\zeta+\mu')^2}\right](2a^2 + \zeta\mu'),\\
\mathcal{R}_1 &= 4i(4a^2 - \delta^2 + 2\zeta\mu')t - 4i(-1)^j\delta\theta + 8, \qquad (12)\\
\mu' &= \pm\frac{1}{\sqrt{2}}[4a^2 - \delta^2 - \sqrt{\delta^2(8a^2+\delta^2)}]^{1/2}
\end{aligned}$$

in the case of $|\delta| < a$. In either case, we set $\theta \equiv 2x + (k_1 + k_2)t$ and $\zeta \equiv (1/\sqrt{2})[\sqrt{\delta^2(8a^2+\delta^2)} + 4a^2 - \delta^2]^{1/2}$. Using the translational symmetry, we shift the above solutions to the origin, to produce compact expressions for them. Note that these PS solutions are nonsingular ones in the entire parameter range.

In addition to the same features which are demonstrated by the conventional PSs, that exist in some multicomponent systems, such as PSs of the bright-dark type, PS doublets, etc., the helicoidal SO coupling can generate more intricate PS structures, among which the most salient aspect is, as shown below, the possibility of having PSs with uniquely large heights.

The consideration of the exact solution (10) reveals that the PS is generally located on top of a periodic background formed by the superposition of two different CWs. The exact solution for the periodic background is

$$\begin{aligned}
|\Psi_1^\mathrm{bg}| &= a\sqrt{1 + \frac{\alpha}{k_\mathrm{m}}\cos\left[(\delta+2k_\mathrm{m})x + \frac{k_1^2-k_2^2}{2}t\right]},\\
|\Psi_2^\mathrm{bg}| &= a\sqrt{1 - \frac{\alpha}{k_\mathrm{m}}\cos\left[(\delta+2k_\mathrm{m})x + \frac{k_1^2-k_2^2}{2}t\right]}. \qquad (13)
\end{aligned}$$

It is moving with speed $v = (k_2^2 - k_1^2)/[2(\delta + 2k_\mathrm{m})]$, where $k_{1,2}$ are the same wavenumbers as in Eq. (8).

Note that, if wavenumbers $k_{1,2}$ and the momentum minimum k_m satisfy the following relationship,

$$k_1 = -k_2 = -k_\mathrm{m}, \tag{14}$$

the cos terms vanish in Eq. (13), i.e., the periodic background degenerates into a flat CW. Due to the presence of the helicoidal SO coupling, the constraint (14) is different from similar ones which provide for the flat background in the coupled-NLSE system [24] and the multicomponent long-wave-short-wave resonance model [60].

PS on the CW background. To reveal the amplification effect of the helicoidal SO coupling on the PS amplitude, we first address the PS solution on top of the flat CW background, subject to constraint (14). The respective background amplitude (13) amounts to

$$|\Psi_1^\mathrm{cw}| = a\sqrt{\frac{k_\mathrm{m}+\alpha}{k_\mathrm{m}}}, \quad |\Psi_2^\mathrm{cw}| = a\sqrt{\frac{k_\mathrm{m}-\alpha}{k_\mathrm{m}}}. \tag{15}$$

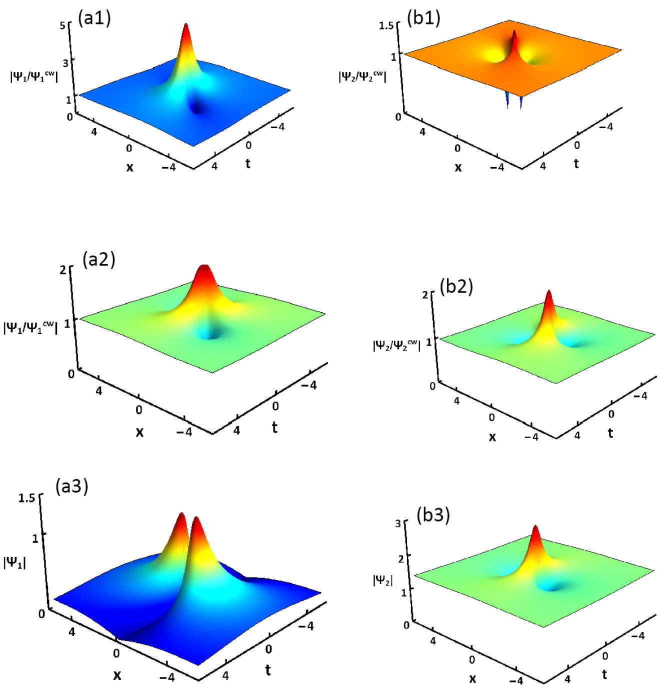

FIG. 1. (a1), (b1) An example of the fundamental PS, produced by solution (10) under condition (14), with the exceptionally high peak amplitude of the Ψ_1 component, for $\alpha = -1/2$, $\kappa = 2/5$. (a2), (b2) generic PS in the Manakov system, for $\alpha = 0$. (a3), (b3) The PS with the zero background in Ψ_1 at $x = 0$, for $\alpha = -1/2$, $\kappa = 0$. The initial amplitude $a = 1$.

Under the action of the SO coupling with strength α, the components of the CW background (15) have different heights.

Taking into regard that the center of the PS solution (10) is pinned to the origin, enhancement factor $|F_j|$ of component Ψ_j is defined as the peak-to-background ratio:

$$F_1 = \frac{\Psi_1(0,0)}{|\Psi_1^{\rm cw}|} = \frac{a\left(\nu_+ f_{u_1} + \nu_- f_{u_2}\right)}{|\Psi_1^{\rm cw}|},$$
$$F_2 = \frac{\Psi_2(0,0)}{|\Psi_2^{\rm cw}|} = \frac{a\left(\nu_- f_{u_1} - \nu_+ f_{u_2}\right)}{|\Psi_2^{\rm cw}|}, \tag{16}$$

where $|\Psi_{1,2}^{\rm cw}|$ are given in Eq. (15), coefficients $\nu_\pm$ are same as in Eq. (6), and factors f_{u_1} and f_{u_2} are defined, for $|\delta| \geqslant a$, as

$$f_{u_1} = 1 - \frac{4\zeta^2}{\zeta^2 + (\delta - \mu)^2}, \quad f_{u_2} = 1 - \frac{4\zeta^2}{\zeta^2 + (\delta + \mu)^2}, \tag{17}$$

and, for $|\delta| < a$, as

$$f_{u_1} = f_{u_2} = 1 - \frac{2(\zeta + \mu')^2}{2a^2 + \zeta\mu'}. \tag{18}$$

Characteristic examples of the PSs featuring large enhancement factors are presented in Fig. 1, which includes a PS with nearly fivefold peak amplitude for the component Ψ_1, with $\alpha = -1/2$ and $\kappa = 2/5$, in Fig. 1(a1). For comparison, two special cases are presented too, viz., for $\alpha = 0$ [Figs. 1(a2) and 1(b2)] and $\kappa = 0$ [Figs. 1(a3) and 1(b3)], which correspond to the Manakov system limit and the uniform SO coupling, respectively. It is observed that, with $\alpha = 0$, the PS amplitudes are only twice as large as those of the background (in fact, for the Manakov system the peak amplitude cannot exceed three times the background value [24]). In addition, for $\kappa = 0$ the PS with zero background in component Ψ_1 or Ψ_2 is produced by Eq. (15), depending on the sign of α. Thus, the helicoidal SO coupling makes it possible to elevate the amplitude of one component to an exceptional level, while suppressing the other component.

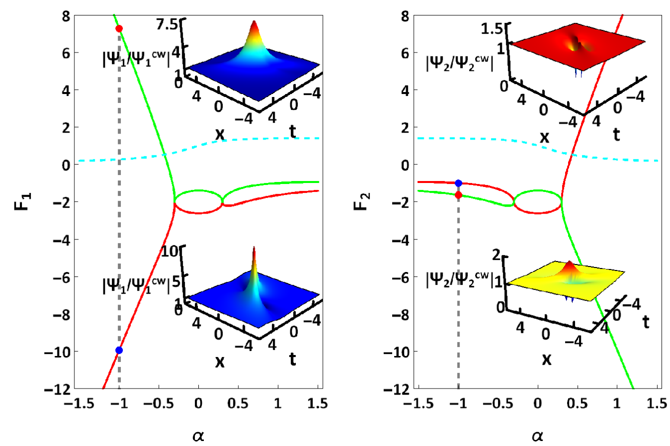

FIG. 2. Enhancement factors F_1 and F_2, as given by Eq. (16) for the PS with the flat background vs the SO-coupling strength α for $a = 1$, $\kappa = 0.4$, $k_1 = -k_2 = -k_{\rm m}$. The red and green curves correspond to μ and μ' taking signs + or − in Eqs. (11) and (12), respectively. The cyan dashed curves show the CW background values $|\Psi_j^{\rm cw}|$, as given by Eq. (15). The insets exhibit the corresponding PSs at $\alpha = -1$.

To further unveil the specific role of the helicoidal SO coupling in generating PSs with exceptionally high amplitudes, we display the dependence of enhancement factors F_j on the SO-coupling strength α and rotation frequency κ in Figs. 2 and 3, respectively. They exhibit an indefinitely large (diverging) enhancement factor for component Ψ_1 or Ψ_2 at $|\alpha| \to \infty$ or $\kappa \to 0$. In particular, the insets to these figures feature the

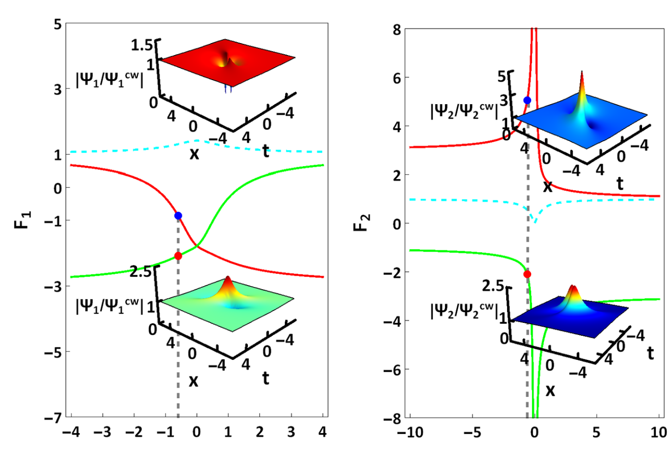

FIG. 3. Enhancement factors F_1 and F_2, as given by Eq. (16), vs. rotation frequency κ [see Eq. (3)] for $a = 1$, $\alpha = 0.6$, $k_1 = -k_2 = -k_{\rm m}$. The red and green curves correspond to μ and μ' taking signs + or − in Eqs. (11) and (12), respectively. The cyan dashed curves show the CW background values $|\Psi_j^{\rm cw}|$, as given by Eq. (15). The insets exhibit the corresponding PSs at $\kappa = -0.6$.

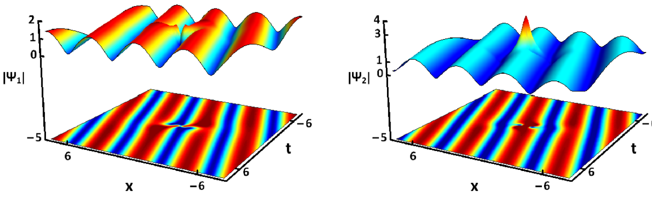

FIG. 4. The PS solution (10) built on top of the periodic background. It exceeds the exceeding threefold enhancement limit, with $k_1 = -k_{\rm m}$ and $k_2 = k_{\rm m} - 3/2$. The other parameters are $a = 1$, $\alpha = -1$, $\kappa = 0.4$.

enhancement factor $|F_1|$ with values close to ten at $\alpha = -1$ and $\kappa = 0.4$, and $|F_2|$ close to five at $\alpha = 0.6$ and $\kappa = -0.6$. A caveat is that the enhancement factor is diverging when the background amplitude $|\Psi_j^{\rm CW}|$ is vanishing, as shown by the cyan dashed curves in Figs. 2 and 3. The absolute values of the PS peak amplitude may be increased by taking values of amplitude $a > 1$ in Eq. (8) (recall it is currently fixed as $a \equiv 1$, by means of scaling).

PSs on top of the periodic background. If the constraint (14) does not hold, the above solution (10) produces the PS built on top of the periodic background. Similar to the case of the flat CW background considered above, we define the enhancement factor to analyze the effect of the helicoidal SO coupling on the PSs. In Fig. 4 we demonstrate a characteristic example exceeding the threefold contrast between the peak amplitude and periodic background in component Ψ_2, for $k_1 = -k_{\rm m}, k_2 = k_{\rm m} - 3/2$.

Next, we address the modulation instability (MI) of the CW field, $\Psi_{j0} = a_j e^{i\mu t}$ with $\mu = a_1^2 + a_2^2$, where a_1 and a_2 are the uniform amplitudes and μ is the chemical potential, in the presence of the helicoidal SO-coupled BECs. To this end, we add small perturbations to the CW fields, viz., $\Psi_j = \Psi_{j0}\{1 + p_j \exp[-i(\beta x - \Omega t)] + q_j^* \exp[i(\beta x - \Omega^* t)]\}$, where β and Ω are, respectively, the real and complex parameters, p_j and q_j being small complex amplitudes. Linearizing the corresponding Eq. (1) with respect to p_j and q_j, we derive a quartic equation for the perturbation eigenfrequency Ω, which determines the MI gain as $\gamma_{\rm h} = |{\rm Im}(\Omega)|_{\rm max}$. In Fig. 5, we display heatmaps for the so found value of γ_h in the (β, α) and (β, κ) parameter planes. The plots reveal that the MI-gain spectra are symmetrically distributed in broad regions of α and κ, which can give rise to the anomalous PS behavior in a broad range of parameters, in comparison to the usual situation underlain by the baseband-MI analysis [61,62]. For instance, Figs. 5(a2) and 5(b2) demonstrate, respectively, that the gain maximum, $\gamma_{\rm h} \approx 1.91$ at $\alpha = -1$ and $\kappa = 0.4$, corresponds to the enhancement factor $|F_1| \approx 10$ in Fig. 2, and the maximum $\gamma_{\rm h} \approx 1.65$, at $\alpha = 0.6$ and $\kappa = -0.6$, corresponds to $|F_2| \approx 5$ in Fig. 3. Such relatively small values of the MI gain, corresponding to the ultrahigh PS peak amplitudes, suggest that these large amplitude values may be relatively easy to attain in the experiment, as the background will not be vulnerable to the quick destruction of the MI-driven blowup, hence these PSs are rather robust modes.

To test the expected robustness of the PSs in the present setting, in Fig. 6 we display results of the numerically simulated evolution of the PSs from Figs. 1(a1) and 1(b1)) under the action of 2% random disturbances. It is observed that the PSs with the ultrahigh amplitudes indeed demonstrate robust propagation.

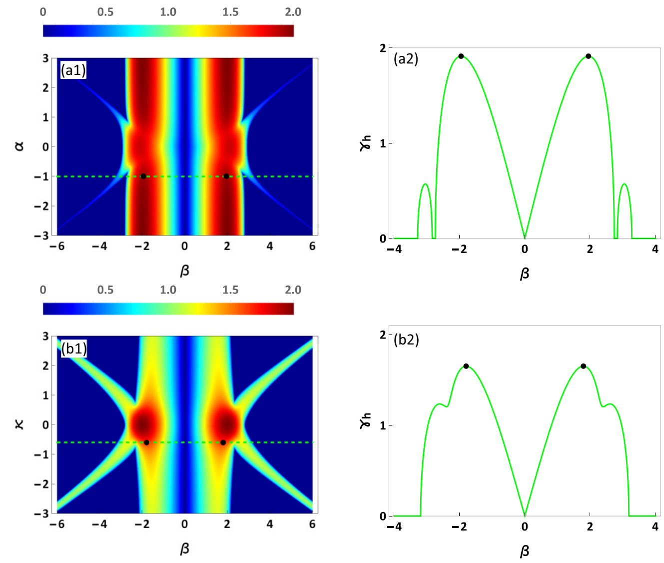

FIG. 5. Heatmaps of the MI gain $\gamma_{\rm h}$ in the (β, α) plane (a1) for $\kappa = 0.4$, and in the (β, κ) plane (b1) for $\alpha = 0.6$. Panels (a2) and (b2) exhibit, respectively, the gain profile $\gamma_{\rm h}$ at $\alpha = -1$ and $\kappa = -0.6$, with the maximum gain marked by black dots. The amplitudes of the underlying CW state are $a_1 = a_2 = 1$.

Conclusion. We have reported the occurrence of abnormal fundamental PSs (Peregrine solitons) with ultrahigh peak amplitudes in the integrable system of GPEs (Gross-Pitaevskii equations), including the helicoidally modulated SO (spin-orbit) coupling, which is a gauge isomer of the Manakov system. The PS solutions are found on top of both the flat and periodic-wave backgrounds. The results demonstrate the existence of RWs [rogue waves with the ultrahigh amplitude in the context of matter waves (BEC)], while previously this was reported in models of nonlinear optics [54,55]. The helicoidal SO coupling is crucially important for generating this abnormal PSs, and the controllable nature of the SO coupling makes the predicted phenomenology experimentally feasible. The MI (modulational instability) is also studied in the system, demonstrating that the high-amplitude PSs readily coexist with moderate MI, thus preventing a strong background instability and improving chances for the experimental creation of the predicted tall rogue waves.

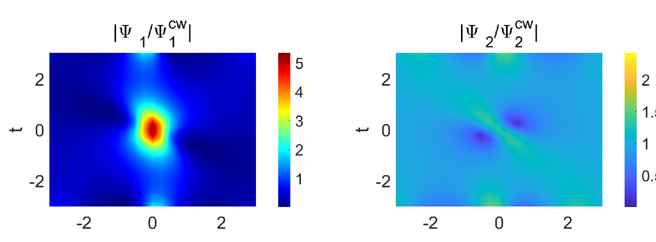

FIG. 6. The result of the numerical simulations of the fundamental PSs from Figs. 1(a1) and 1(b1) under the action of the 2% noise.

Acknowledgments. This work was supported by the National Natural Science Foundation of China (Grant No. 11975172) and the Natural Science Foundation of Hubei Province of China (Grant No. 2023AFB222). The work of B.A.M. is supported, in part, by the Israel Science Foundation (Grant No. 1695/22).

[1] K. Dysthe, H. E. Krogstad, and P. Müller, Oceanic rogue waves, Annu. Rev. Fluid Mech. **40**, 287 (2008).
[2] C. Kharif, E. Pelinovsky, and A. Slunyaev, *Rogue Waves in the Ocean* (Springer-Verlag, Berlin, 2009).
[3] A. Chabchoub, N. P. Hoffmann, and N. Akhmediev, Rogue wave observation in a water wave tank, Phys. Rev. Lett. **106**, 204502 (2011).
[4] A. Chabchoub, N. Hoffmann, M. Onorato, A. Slunyaev, A. Sergeeva, E. Pelinovsky, and N. Akhmediev, Observation of a hierarchy of up to fifth-order rogue waves in a water tank, Phys. Rev. E **86**, 056601 (2012).
[5] A. Chabchoub, N. Hoffmann, M. Onorato, and N. Akhmediev, Super rogue waves: Observation of a higher-order breather in water waves, Phys. Rev. X **2**, 011015 (2012).
[6] J. M. Dudley, G. Genty, A. Mussot, A. Chabchoub, and F. Dias, Rogue waves and analogies in optics and oceanography, Nat. Rev. Phys. **1**, 675 (2019).
[7] D. R. Solli, C. Ropers, P. Koonath, and B. Jalali, Optical rogue waves, Nature (London), **450**, 1054 (2007).
[8] C. Lecaplain, P. Grelu, J. M. Soto-Crespo, and N. Akhmediev, Dissipative rogue waves generated by chaotic pulse bunching in a mode-locked laser, Phys. Rev. Lett. **108**, 233901 (2012).
[9] W. R. Sun, B. Tian, Y. Jiang, and H. L. Zhen, Optical rogue waves associated with the negative coherent coupling in an isotropic medium, Phys. Rev. E **91**, 023205 (2015).
[10] S. H. Chen, J. M. Soto-Crespo, F. Baronio, P. Grelu, and D. Mihalache, Rogue-wave bullets in a composite (2+1)D nonlinear medium, Opt. Express **24**, 15251 (2016).
[11] H. Bailung, S. K. Sharma, and Y. Nakamura, Observation of Peregrine solitons in a multicomponent plasma with negative ions, Phys. Rev. Lett. **107**, 255005 (2011).
[12] Y. V. Bludov, V. V. Konotop, and N. Akhmediev, Matter rogue waves, Phys. Rev. A **80**, 033610 (2009).
[13] A. Romero-Ros, G. C. Katsimiga, S. I. Mistakidis, B. Prinari, G. Biondini, P. Schmelcher, and P. G. Kevrekidis, Theoretical and numerical evidence for the potential realization of the Peregrine soliton in repulsive two-component Bose-Einstein condensates, Phys. Rev. A **105**, 053306 (2022).
[14] A. Romero-Ros, G. C. Katsimiga, S. I. Mistakidis, S. Mossman, G. Biondini, P. Schmelcher, P. Engels, and P. G. Kevrekidis, Experimental realization of the Peregrine soliton in repulsive two-component Bose-Einstein condensates, Phys. Rev. Lett. **132**, 033402 (2024).
[15] W. R. Sun, B. Tian, H. L. Zhen, and Y. Sun, Breathers and rogue waves of the fifth-order nonlinear Schrödinger equation in the Heisenberg ferromagnetic spin chain, Nonlin. Dyn. **81**, 725 (2015).
[16] Z. Y. Yan, Financial rogue waves, Commun. Theor. Phys. **54**, 947 (2010).
[17] Z. Y. Yan, Nonautonomous “rogons” in the inhomogeneous nonlinear Schrödinger equation with variable coefficients, Phys. Lett. A **374**, 672 (2010).
[18] Z. Yan, V. V. Konotop, and N. Akhmediev, Three-dimensional rogue waves in nonstationary parabolic potentials, Phys. Rev. E **82**, 036610 (2010).
[19] S. W. Xu, J. S. He, and L. H. Wang, The Darboux transformation of the derivative nonlinear Schrödinger equation, J. Phys. A: Math. Theor. **44**, 305203 (2011).
[20] Y. S. Tao and J. S. He, Multisolitons, breathers, and rogue waves for the Hirota equation generated by the Darboux transformation, Phys. Rev. E **85**, 026601 (2012).
[21] J. S. He, H. R. Zhang, L. H. Wang, K. Porsezian, and A. S. Fokas, Generating mechanism for higher-order rogue waves, Phys. Rev. E **87**, 052914 (2013).
[22] K. Wing Chow, H. N. Chan, D. J. Kedziora, and R. H. J. Grimshaw, Rogue wave modes for the long wave-short wave resonance model, J. Phys. Soc. Jpn. **82**, 074001 (2013).
[23] H. N. Chan, K. W. Chow, D. J. Kedziora, R. H. J. Grimshaw, and E. Ding, Rogue wave modes for a derivative nonlinear Schrödinger model, Phys. Rev. E **89**, 032914 (2014).
[24] S. Chen and D. Mihalache, Vector rogue waves in the Manakov system: Diversity and compossibility, J. Phys. A: Math. Theor. **48**, 215202 (2015).
[25] J. G. Rao, K. W. Chow, D. Mihalache, and J. S. He, Completely resonant collision of lumps and line solitons in the Kadomtsev-Petviashvili I equation, Stud. Appl. Math. **147**, 1007 (2021).
[26] L. Liu, W.-R. Sun, and B. A. Malomed, Formation of rogue waves and modulational instability with zero-wavenumber gain in multi-component systems with coherent coupling, Phys. Rev. Lett. **131**, 093801 (2023).
[27] D. H. Peregrine, Water waves, nonlinear Schrödinger equations and their solutions, J. Aust. Math. Soc. Ser. B **25**, 16 (1983).
[28] A. Tikan, C. Billet, G. El, A. Tovbis, M. Bertola, T. Sylvestre, F. Gustave, S. Randoux, G. Genty, P. Suret, and J. M. Dudley, Universality of the Peregrine soliton in the focusing dynamics of the cubic nonlinear Schrödinger equation, Phys. Rev. Lett. **119**, 033901 (2017).
[29] B. Kibler, J. Fatome, C. Finot, G. Millot, F. Dias, G. Genty, N. Akhmediev, and J. M. Dudley, The Peregrine soliton in nonlinear fibre optics, Nat. Phys. **6**, 790 (2010).
[30] G. Michel, F. Bonnefoy, G. Ducrozet, G. Prabhudesai, A. Cazaubiel, F. Copie, A. Tikan, P. Suret, S. Randoux, and E. Falcon, Emergence of Peregrine solitons in integrable turbulence of deep water gravity waves, Phys. Rev. Fluids **5**, 082801(R) (2020).
[31] Y. J. Lin, K. Jiménez-García, and I. B. Spielman, Spin-orbit-coupled Bose-Einstein condensates, Nature (London) **471**, 83 (2011).
[32] V. Galitski and I. B. Spielman, Spin-orbit coupling in quantum gases, Nature (London) **494**, 49 (2013).
[33] C. Hamner, Y. Zhang, M. A. Khamehchi, M. J. Davis, and P. Engels, Spin-orbit-coupled Bose-Einstein condensates in a one-dimensional optical lattice, Phys. Rev. Lett. **114**, 070401 (2015).

[34] H. Zhai, Degenerate quantum gases with spin–orbit coupling: A review, Rep. Prog. Phys. **78**, 026001 (2015).
[35] Y. Zhang, M. E. Mossman, T. Busch, P. Engels, and C. Zhang, Properties of spin–orbit-coupled Bose–Einstein condensates, Front. Phys. **11**, 118103 (2016).
[36] J. Dalibard, F. Gerbier, G. Juzeliūnas, and P. Ö hberg, Colloquium: Artificial gauge potentials for neutral atoms, Rev. Mod. Phys. **83**, 1523 (2011).
[37] J. Ruseckas, G. Juzeliūnas, P. Öhberg, and M. Fleischhauer, Non-Abelian gauge potentials for ultracold atoms with degenerate dark states, Phys. Rev. Lett. **95**, 010404 (2005).
[38] J. Struck, C. Ölschläger, M. Weinberg, P. Hauke, J. Simonet, A. Eckardt, M. Lewenstein, K. Sengstock, and P. Windpassinger, Tunable gauge potential for neutral and spinless particles in driven optical lattices, Phys. Rev. Lett. **108**, 225304 (2012).
[39] Y. Zhang, G. Chen, and C. Zhang, Tunable spin-orbit coupling and quantum phase transition in a trapped Bose-Einstein condensate, Sci. Rep. **3**, 1937 (2013).
[40] K. Jiménez-García, L. J. LeBlanc, R. A. Williams, M. C. Beeler, C. Qu, M. Gong, C. Zhang, and I. B. Spielman, Tunable spin-orbit coupling via strong driving in ultracold-atom systems, Phys. Rev. Lett. **114**, 125301 (2015).
[41] X. Luo, L. Wu, J. Chen, Q. Guan, K. Gao, Z.-F. Xu, L. You, and R. Wang, Tunable atomic spin-orbit coupling synthesized with a modulating gradient magnetic field, Sci. Rep. **6**, 18983 (2016).
[42] S. S. S. Hejazi, J. Polo, R. Sachdeva, and T. Busch, Symmetry breaking in binary Bose-Einstein condensates in the presence of an inhomogeneous artificial gauge field, Phys. Rev. A **102**, 053309 (2020).
[43] Y. V. Kartashov, V. V. Konotop, and D. A. Zezyulin, Bose-Einstein condensates with localized spin-orbit coupling: Soliton complexes and spinor dynamics, Phys. Rev. A **90**, 063621 (2014).
[44] Y. V. Kartashov and V. V. Konotop, Solitons in Bose-Einstein condensates with helicoidal spin-orbit coupling, Phys. Rev. Lett. **118**, 190401 (2017).
[45] Y. V. Kartashov, E. Sherman, B. Malomed, and V. Konotop, Stable two-dimensional soliton complexes in Bose-Einstein condensates with helicoidal spin-orbit coupling, New J. Phys. **22**, 103014 (2020).
[46] Y. Li, X. Zhang, R. Zhong, Z. Luo, B. Liu, C. Huang, W. Pang, and B. A. Malomed, Two-dimensional composite solitons in Bose-Einstein condensates with spatially confined spin-orbit coupling, Commun. Nonlin. Sci. Num. Sim. **73**, 481 (2019).
[47] B. Liu, R. Zhong, Z. Chen, X. Qin, H. Zhong, Y. Li, and B. A. Malomed, Holding and transferring matter-wave solitons against gravity by spin-orbit-coupling tweezers, New J. Phys. **22**, 043004 (2020).
[48] M. C. Rechtsman, J. M. Zeuner, Y. Plotnik, Y. Lumer, D. Podolsky, F. Dreisow, S. Nolte, M. Segev, and A. Szameit, Photonic Floquet topological insulators, Nature (London) **496**, 196 (2013).
[49] Y. V. Kartashov, V. V. Konotop, M. Modugno, and E. Ya. Sherman, Solitons in inhomogeneous gauge potentials: Integrable and nonintegrable dynamics, Phys. Rev. Lett. **122**, 064101 (2019).
[50] F. Baronio, A. Degasperis, M. Conforti, and S. Wabnitz, Solutions of the vector nonlinear Schrödinger equations: Evidence for deterministic rogue waves, Phys. Rev. Lett. **109**, 044102 (2012).
[51] S. V. Manakov, On the theory of two-dimensional stationary self-focusing of electromagnetic waves, Sov. Phys. JETP **38**, 248 (1974).
[52] F. Baronio, M. Conforti, A. Degasperis, and S. Lombardo, Rogue waves emerging from the resonant interaction of three waves, Phys. Rev. Lett. **111**, 114101 (2013).
[53] S. Chen, F. Baronio, J. M. Soto-Crespo, Ph. Grelu, M. Conforti, and S. Wabnitz, Optical rogue waves in parametric three-wave mixing and coherent stimulated scattering, Phys. Rev. A **92**, 033847 (2015).
[54] S. Chen, Y. Ye, J. M. Soto-Crespo, P. Grelu, and F. Baronio, Peregrine solitons beyond the threefold limit and their two-soliton interactions, Phys. Rev. Lett. **121**, 104101 (2018).
[55] S. Chen, C. Pan, P. Grelu, F. Baronio, and N. Akhmediev, Fundamental peregrine solitons of ultrastrong amplitude enhancement through self-steepening in vector nonlinear systems, Phys. Rev. Lett. **124**, 113901 (2020).
[56] X. X. Li, R. J. Cheng, A. X. Zhang, and J. K. Xue, Modulational instability of Bose-Einstein condensates with helicoidal spin-orbit coupling, Phys. Rev. E **100**, 032220 (2019).
[57] X. X. Li, R. J. Cheng, J. L. Ma, A. X. Zhang, and J. K. Xue, Solitary matter wave in spin-orbit-coupled Bose-Einstein condensates with helicoidal gauge potential, Phys. Rev. E **104**, 034214 (2021).
[58] S. V. Samsonov, A. D. R. Phelps, V. L. Bratman, G. Burt, G. G. Denisov, A. W. Cross, K. Ronald, W. He, and H. Yin, Compression of frequency-modulated pulses using helically corrugated waveguides and its potential for generating multigigawatt rf radiation, Phys. Rev. Lett. **92**, 118301 (2004).
[59] G. Burt, S. V. Samsonov, K. Ronald, G. G. Denisov, A. R. Young, V. L. Bratman, A. D. R. Phelps, A. W. Cross, I. V. Konoplev, W. He, J. Thomson, and C. G. Whyte, Dispersion of helically corrugated waveguides: Analytical, numerical, and experimental study, Phys. Rev. E **70**, 046402 (2004).
[60] S. Chen, J. M. Soto-Crespo, and P. Grelu, Coexisting rogue waves within the (2+1)-component long-wave–short-wave resonance, Phys. Rev. E **90**, 033203 (2014).
[61] F. Baronio, M. Conforti, A. Degasperis, S. Lombardo, M. Onorato, and S. Wabnitz, Vector rogue waves and baseband modulation instability in the defocusing regime, Phys. Rev. Lett. **113**, 034101 (2014).
[62] F. Baronio, S. Chen, Ph. Grelu, S. Wabnitz, and M. Conforti, Baseband modulation instability as the origin of rogue waves, Phys. Rev. A **91**, 033804 (2015).